Electronic Supporting Information for: Controlling Amphipathic Peptide Adsorption by Smart Switchable Germanium Interfaces

Laura-Marleen Baumgartner[a] Andreas Erbe[a,b] Aimee L. Boyle[c] Martin Rabe*[a]

[a] Max-Planck-Institut für Eisenforschung GmbH, Max-Planck-Str. 1, 40237 Düsseldorf, Germany
[b] Department of Materials Science and Engineering, NTNU, Norwegian University of Science and Technology, 7491 Trondheim, Norway
[c] Leiden Institute of Chemistry, Leiden University, Einsteinweg 55, 2333 CC Leiden, The Netherlands
∗ Corresponding author: m.rabe@mpie.de

Contents

1 Supporting spectroscopic data and analysis

1.1 Experiments without peptides

The potential dependent p-polarised spectra of Ge in the range −0.19 V to −1.19 V vs. SHE show several features (ESI-Fig. 1). The development of a broad negative band around 2500 cm^{-1} including a positive feature at 2660 cm^{-1} is assigned to the OD stretching vibrations (ν_{OD}). A detailed analysis of the structural changes observed in the analogous OH stretching mode region is available elsewhere [1, 2]. Here, an increase of the OH stretching vibration centered at 3400 cm^{-1} is observed over the full negative and positive scan. At first approximation this OH stretching band increases independently of the applied potential, which indicates a slow introduction of H_2O into the buffer, probably caused by residual vapor in the inert gas purge or from the reference electrode electrolyte filling. The negative feature centered at ca. 1210 cm^{-1} developing during the scan is assigned to the D_2O bending mode. The origin of a sharp potential dependent band at 1560 cm^{-1} is not fully clear. The broad bands in the range 1400 cm^{-1} to 1500 cm^{-1} are assigned to the Ge−D_1 and Ge−D_2 stretching vibrations based on comparison with reference values listed in ESI-Table 1. However, also contributions from an HDO bending

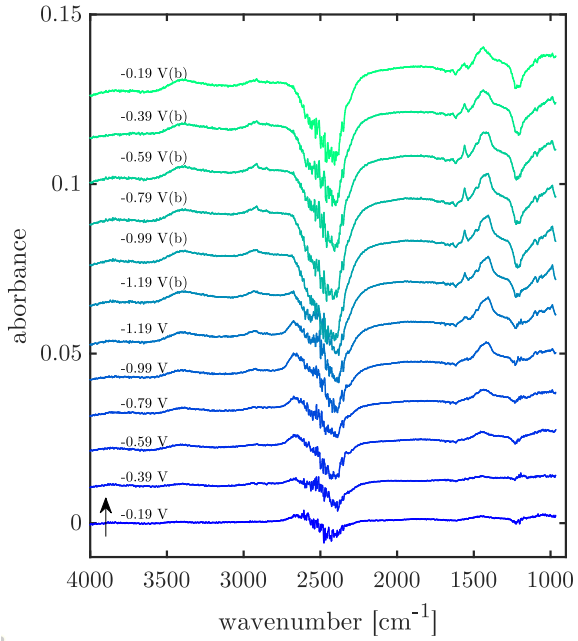

ESI-Fig. 1: Potential dependent ATR-IR p-polarized spectra of bare Ge (100) in d-PB pD 7.4. Spectra are offset for clarity, arrow indicates initial spectrum and scan direction.

might arise at ca. 1460 cm^{-1} [3] due to residual H and the increasing amount of H in the system.

Multivariate curve resolution analysis of Ge-D bands

A singular value decomposition-based matrix least square (SVD-MLS) approach was used to deconvolute the spectral region of the Ge-D stretching vibrations to evaluate the progression of the different contributions during the negative scan (ESI-Figs. 2 & 3) and the subsequent positive scan (ESI-Figs. 4 & 5). By means of this method the matrix $\mathbf{A}$ containing in its columns the potential dependent, linear baseline corrected absorbance peaks is deconvoluted into two matrices $\mathbf{D}$ and $\mathbf{F}$ for which applies:

$$\mathbf{A} = \mathbf{D}\mathbf{F}^{\mathrm{T}}. \tag{1}$$

To do so, transition models ($f(E)_i$) describing the potential (E) dependency of the spectral components in the i^{th} column of $\mathbf{F}$ ($\mathbf{F_i}$) must be chosen. Then, $\mathbf{D}$ can be determined by application of the SVD-MLS algorithm detailed in [4] and implemented in [5]. The data sets for positive and negative scan and s- and p-polarisation were analysed separately using a rank of 3 or 4 for the SVD. Sigmoidal functions were used as empirical descriptions for the transitions in $\mathbf{F}$:

$$f(E)_i = b_i + \frac{m_i - b_i}{1 + \exp\left(\frac{E_{\mathrm{m},i} - E}{\delta_i}\right)}. \tag{2}$$

Here, the subscript denotes the i^{th} transition, b is the minimum value, m the maximum value, δ the width and E_{m} the midpoint of the transition. For particular data sets (positive scan, p-polarisation cf. ESI-fig. 4 and negative scan, s-polarisation cf. ESI-fig. 3) a transition model with two linear domains was found to more reasonably describe the F_1 component:

$$f(E)_i = \begin{cases} m_{\mathrm{a},i}(E - E_{\mathrm{int}}) + y_{\mathrm{int}} & (E \leq E_{\mathrm{int}}) \\ m_{\mathrm{b},i}(E - E_{\mathrm{int}}) + y_{\mathrm{int}} & (E > E_{\mathrm{int}}) \end{cases}, \tag{3}$$

with the slopes m_{a} and m_{b} of two linear functions intersecting at $(E_{\mathrm{int}}; y_{\mathrm{int}})$. The bounds for the MLS routine have been chosen in a way that the values in $\mathbf{F}_i$ increase between 0 and 1 in the scan direction except for the base components for which $\mathbf{F}_i = 1$ at all potentials.

In general it was found that two spectral transitions ($\mathbf{F}_{1,2}$ and $\mathbf{D}_{1,2}$ in ESI-Figs. 2 - 5) and a base spectrum ($\mathbf{F}_3 = 1$ and $\mathbf{D}_3$ in ESI-Figs. 2 - 5) sufficiently describe the observable spectral changes. In all datasets $\mathbf{D}_{1,2}$ are found to be well separated spectral components with independent transitions in $\mathbf{F}$.

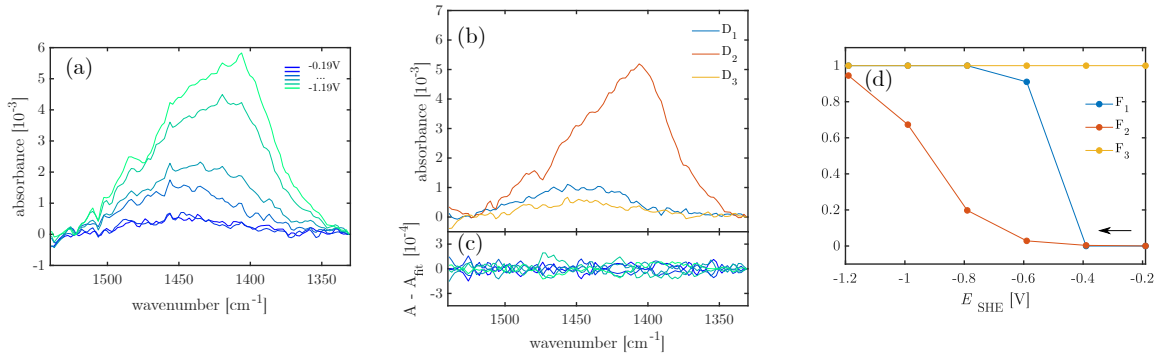

ESI-Fig. 2: Results of SVD-MLS deconvolution applied to potential dependent (negative scan) ATR-IR p-polarized spectra of bare Ge (100) in d-PB pD 7.4. (a) Absorbance spectra after baseline correction (rows of $\mathbf{A}$); (b) spectral components $\mathbf{D}_{1,2,3}$; (c) residuals of the fitted model, compared to the original data, the color scale is equivalent to (a); (d) potential dependent transitions $\mathbf{F}_{1,2,3}$ associated to the respective spectral components D in (b). The arrow in (d) indicates the scan direction.

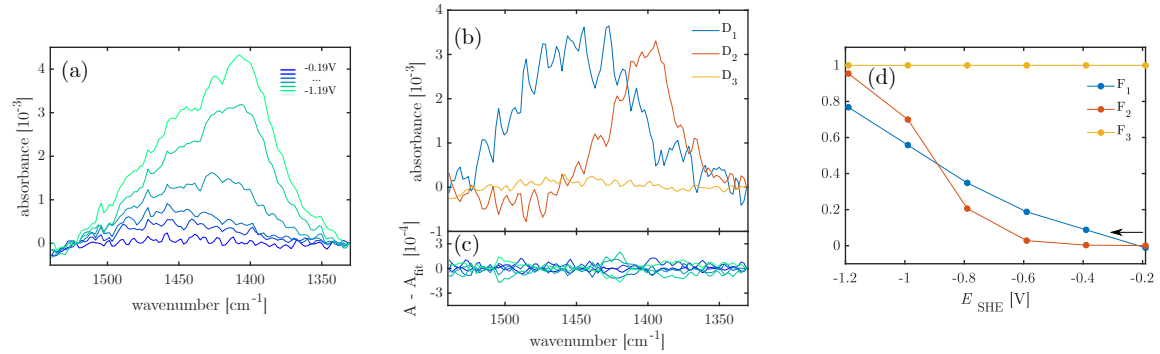

ESI-Fig. 3: Results of SVD-MLS deconvolution applied to potential dependent (negative scan) ATR-IR s-polarized spectra of bare Ge (100) in d-PB pD 7.4. (a) Absorbance spectra after baseline correction (rows of $\mathbf{A}$); (b) spectral components $\mathbf{D}_{1,2,3}$; (c) residuals of the fitted model compared to the original data, the color scale is equivalent to (a); (d) potential dependent transitions $\mathbf{F}_{1,2,3}$ associated to the respective spectral components D in (b). The arrow in (d) indicates the scan direction.

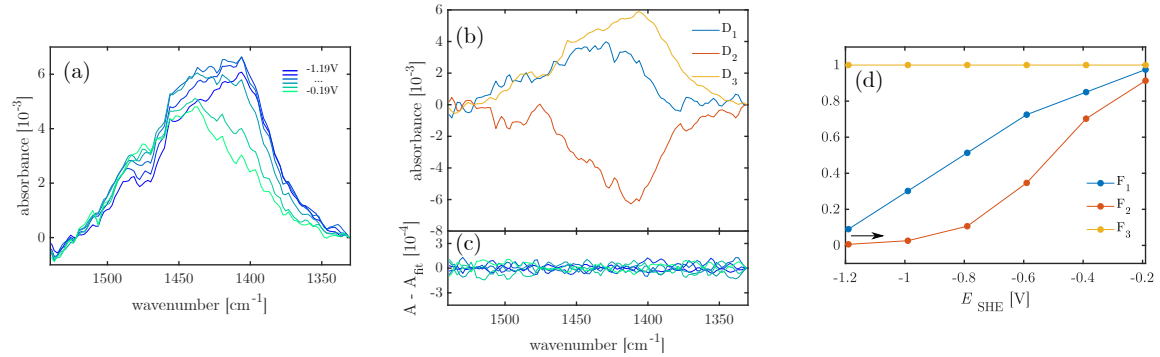

ESI-Fig. 4: Results of SVD-MLS deconvolution applied to potential dependent (positive scan) ATR-IR p-polarized spectra of bare Ge (100) in d-PB pD 7.4. (a) Absorbance spectra after baseline correction (rows of $\mathbf{A}$); (b) spectral components $\mathbf{D}_{1,2,3}$; (c) residuals of the fitted model compared to the original data, the color scale is equivalent to (a); (d) potential dependent transitions $\mathbf{F}_{1,2,3}$ associated to the respective spectral components D in (b). The arrow in (d) indicates the scan direction.

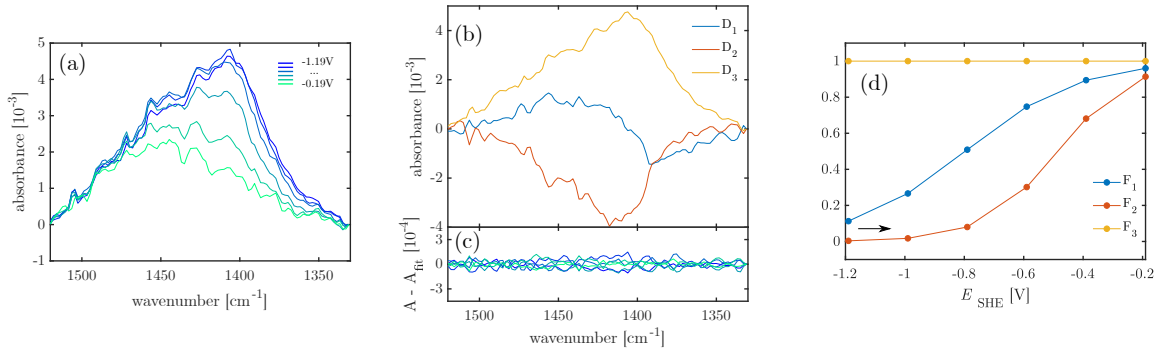

ESI-Fig. 5: Results of SVD-MLS deconvolution applied to potential dependent (positive scan) ATR-IR s-polarized spectra of bare Ge (100) in d-PB pD 7.4. (a) Absorbance spectra after baseline correction (rows of $\mathbf{A}$); (b) spectral components $\mathbf{D}_{1,2,3}$; (c) residuals of the fitted model compared to the original data, the color scale is equivalent to (a); (d) potential dependent transitions $\mathbf{F}_{1,2,3}$ associated to the respective spectral components D in (b). The arrow in (d) indicates the scan direction.

Interpretation of component $\mathbf{D}_1$

The $\mathbf{D}_1$ components show broad bands centered around 1430 cm^{-1} to 1450 cm^{-1} that are positive during positive and negative scans (ESI-Figs. 2 - 5 b). By definition, all transitions $\mathbf{F}_{1,2}$ increase in the scanning direction, hence the spectral components being positive means they represent an irreversible increasing absorbance over the whole course of the experiment. Accordingly, the $\mathbf{D}_1$ components are assigned to HOD bending vibrations (δ_{HOD}), arising from protons carried in from residual humidity in the atmosphere or other sources.

Interpretation of component $\mathbf{D}_2$

The $\mathbf{D}_2$ spectra show positive peaks during negative scans and negative peaks during positive scans centered at 1395 cm^{-1} to 1418 cm^{-1} and with shoulders on the high wavenumber side at ca. 1433 cm^{-1} to 1454 cm^{-1}. Thus, they indicate an increasing absorbance during negative scan that is reversible upon positive scan. The positions of the maxima and the shoulder are well in range with the wavenumbers expected from the maximum possible isotope shifted (shift by a factor of $\frac{1}{\sqrt{2}}$) stretching vibrations of GeH_1 and GeH_2 (cf. ESI-Table 1). Accordingly they are assigned to GeD_1 and GeD_2 stretching vibrations and the $\mathbf{D}_1$ component can be understood as a combination of these bands and is labeled ν_{GeD} in the main part of the manuscript. So far, direct observation of interface Ge-D bands has been reported from UHV experiments only, which yielded comparable results.[6, 7]. However, the assignment of the high frequency shoulders at 1433 cm^{-1} to 1454 cm^{-1} to GeD_2 should be taken with care. Alternatively it may be assigned to an DO-Ge-Ge-D mixed intermediate, based on the data reported in [8]. Furthermore, because of some overlap with the $\mathbf{D}_1$ component it remains unclear whether the deconvolution yields perfectly separated components and hence the shoulder in $\mathbf{D}_2$ may originate from remainders of the HOD spectrum. A more certain assignment might be obtained by SVD-MLS analysis of data with higher potential resolution which is however not in the scope of the current work. However, the above discussion shows that for the determination of the deuteration state of the interface the absorbance of the main peak at 1395 cm^{-1} to 1418 cm^{-1} can be employed because it can clearly be assigned to the GeD_1 species. The absorbance at 1405 cm^{-1} is therefore used in the main part of the paper to spectroscopically monitor

ESI-Table 1: Reference values and assignments for Ge-H/Ge-D stretching modes observed on Ge(100) and (111) as well as expected Ge-D wavenumbers by isotope shift, ordered by publication date (newest first).

[Ref]	Ge surface	assignment	$\tilde{\nu}$ [cm^{-1}]	$\frac{1}{\sqrt{2}}\tilde{\nu}$ [cm^{-1}]	remark/condition
[2]	(100)	GeH_2	2025	1432	in situ electrochem.
		GeH_1	1965	1390	
[8]	(100) & (111)	HO−Ge−Ge−H or HOGe−H	2025 - 2030	1432 - 1435	in situ electrochem.
		GeH_2	2001 - 2017	1415 - 1426	
		GeH_1	1977 - 1983	1398 - 1402	
[9]	(100)	GeH_3	2060	1457	HF treated interface
		GeH_2	2020	1428	
		GeH_1	1987	1405	
[10–12]	(100) & (111)	GeH_2	2020	1428	in situ electrochem.
		GeH_1	1950 - 1990	1379 - 1407	
[6]	(111)	GeH_3	2060	1457	UHV, 500 K
		GeH_2	2021	1429	
		GeH_1	1971	1394	
		GeD_1	1423	-	
[7]	(100)	ν_{as} H−GeGe−H	1979	1399	UHV
		ν_s H−GeGe−H	1991	1408	
		Ge−D	1430	-	
		Ge−D	1437	-	

the deuteration state of the Ge interface.

Correcting spectra for δ_{HOD}

The measured potential dependent spectra can be corrected for the irreversible HOD contribution by applying eq. (1) while omitting $\mathbf{D}_1$ and $\mathbf{F}_1$. Based on the assignment above the resulting p-polarized spectra shown in ESI-Fig. 6 can be understood as the potential dependent pure GeD spectra. It highlights the reversibility of the surface transformation in the deuterated buffer used for the experiments. The corrected absorbance of the GeD band at 1405 cm^{-1} is plotted along with the CV in Figure 1a in the main text and discussed there.

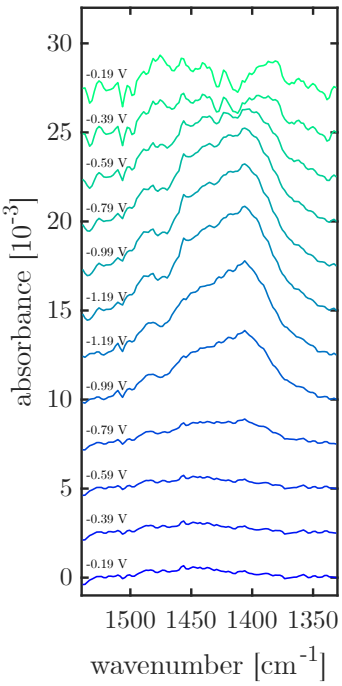

ESI-Fig. 6: Potential dependent ATR-IR spectra in p-polarisation corrected for the increasing contribution of the δ_{HOD} vibration, i.e. of $\mathbf{D}_1$ and $\mathbf{F}_1$.

1.2 Experiments with peptides

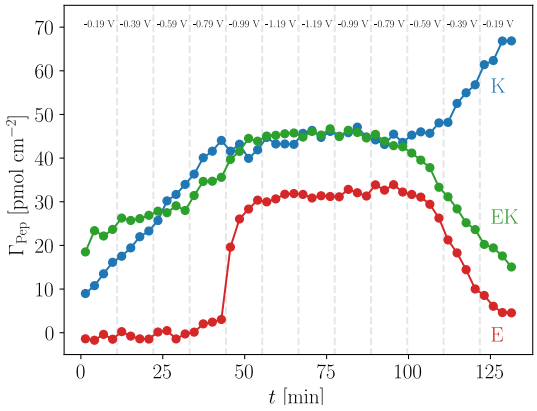

ESI-Fig. 7: Time dependency of peptide surface concentration during potential scans.

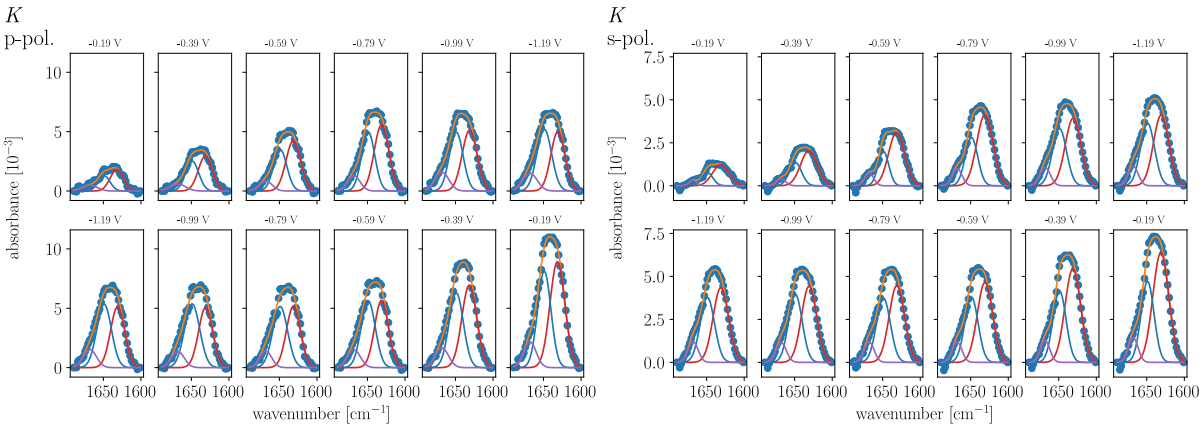

ESI-Fig. 8: Results of the automated peak fitting routine for **K** in p- and s-polarisation. Three Gaussians were used to fit the band shapes after subtraction of a linear baseline.

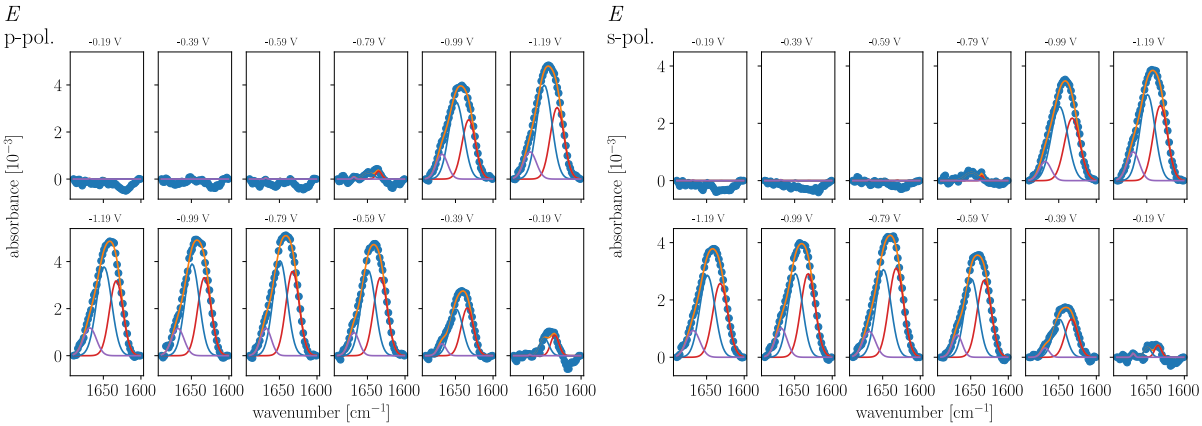

ESI-Fig. 9: Results of automated peak fitting routine for **E** in p- and s-polarisation. Three Gaussians were used to fit the band shapes after subtraction of a linear baseline.

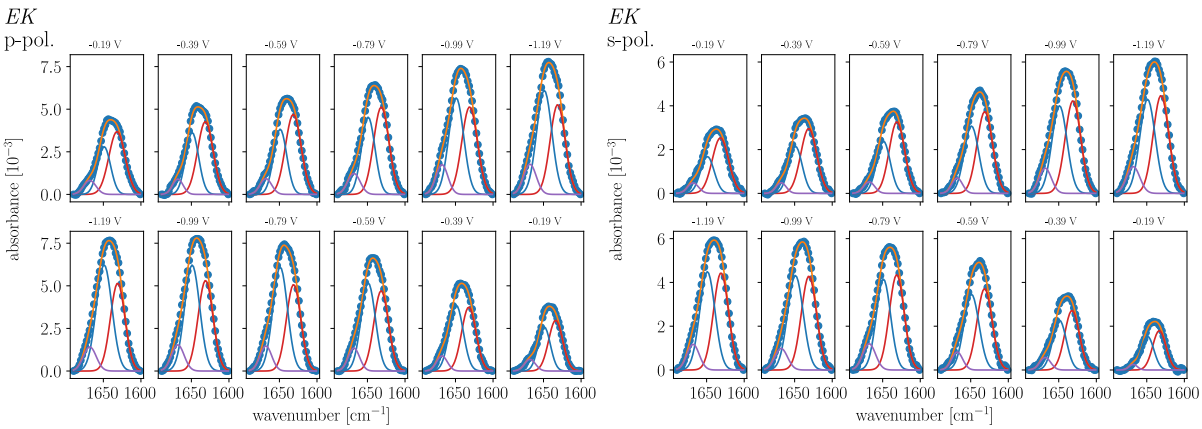

ESI-Fig. 10: Results of automated peak fitting routine for **EK** in p- and s-polarisation. Three Gaussians were used to fit the band shapes after subtraction of a linear baseline.

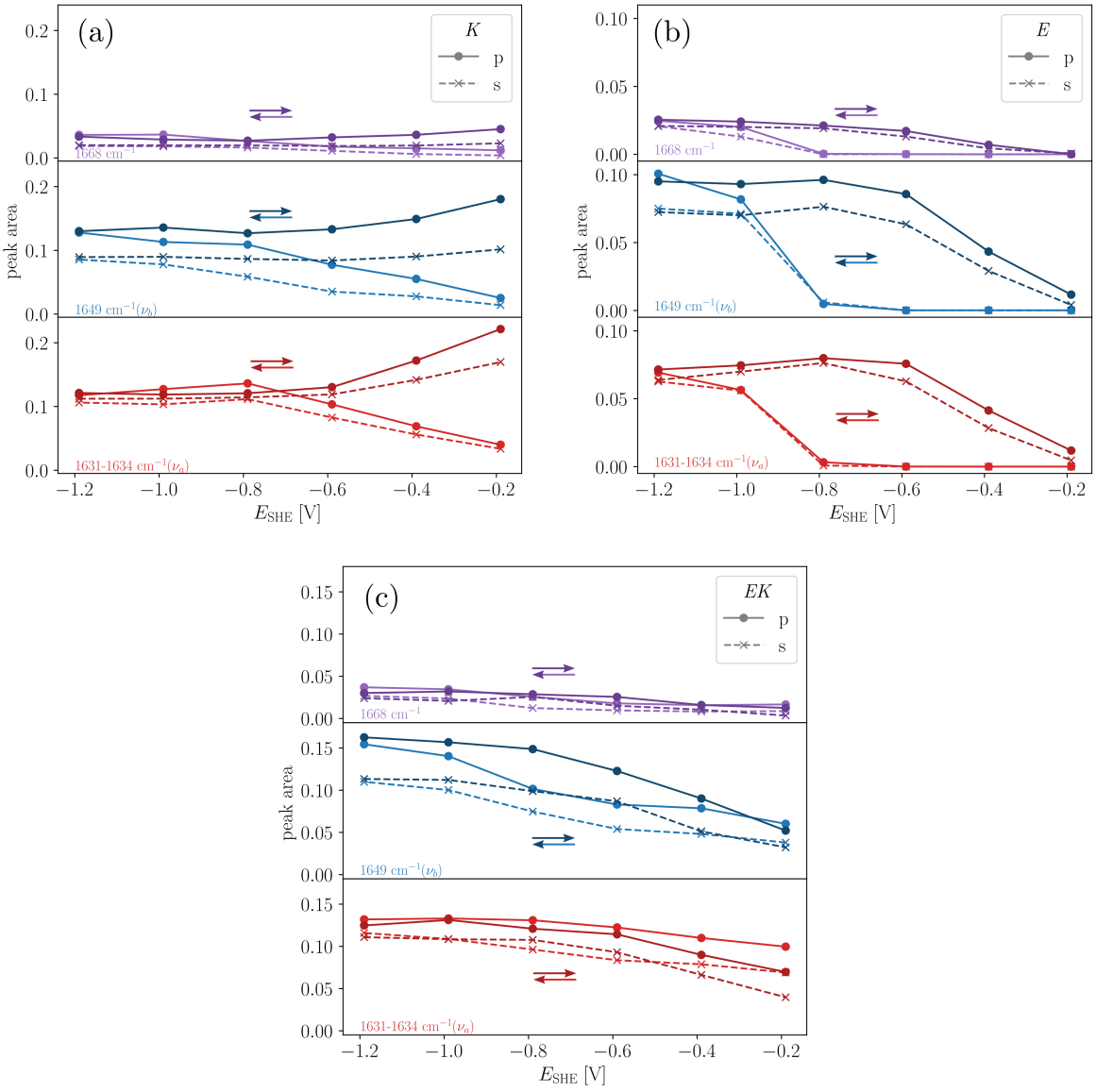

ESI-Fig. 11: Results of automated peak fitting routine. Peak areas of single components for (a): **K**; (b): **E**; (c): **EK**.

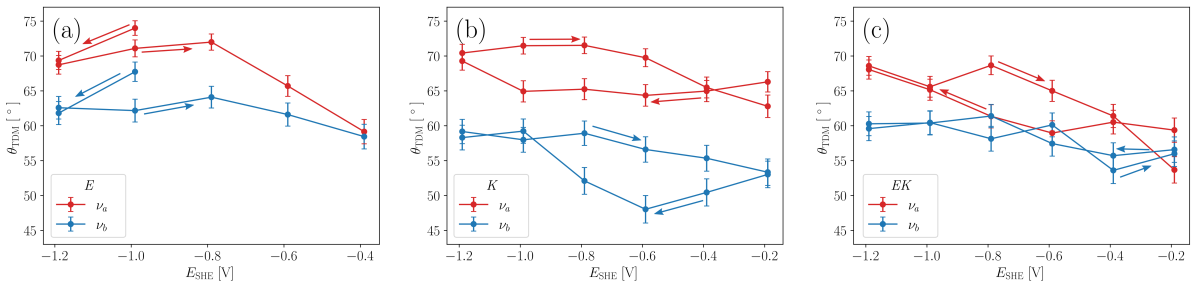

ESI-Fig. 12: Angles between surface normal and transition dipole moments of the major peak components ν_a at ca. 1630 cm^{-1} and ν_b at 1649 cm^{-1} determined by peak fitting. Peptides: (a): **E**; (b): **K**; (c): **EK**.

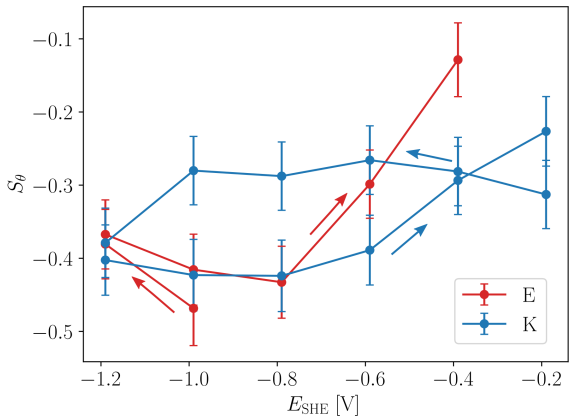

ESI-Fig. 13: Potential dependent order parameters of **E** and **K** determined from ν_a with $\alpha = (20 \pm 5)^\circ$.

2 Parameters for quantitative spectra analysis

ESI-Table 2: Parameters used for quantitative spectra analysis.

parameter	value	explanation & source
n_{peptide}	1.45 ± 0.05	Refractive index of peptide layer assumed to be similar to globular protein (HSA)[13]
$n_{\mathrm{D_2O}}$	Amide I': 1.3375 ± 0.0025; Ge-D ($1405\,\mathrm{cm^{-1}}$): 1.3193 ± 0.0005	Refractive index of D_2O from Max and Chapados [14]
n_{Ge}	Amide I': 4.0107 ± 0.0005 ; Ge-D ($1405\,\mathrm{cm^{-1}}$): $4.007\,84 \pm 0.000\,03$	Refractive index of Ge from Sellmeier model by Burnett et al. [15]
θ	$(45.0 \pm 1.0)^\circ$	IR beam incident angle from crystal geometry
l	$(52.0 \pm 0.1)\,\mathrm{mm}$	Length of Ge IRE as specified by manufacturer
h	$(0.50 \pm 0.05)\,\mathrm{mm}$	Thickness of Ge IRE as specified by manufacturer
l_{c}	$(13.0 \pm 0.1)\,\mathrm{mm}$	Length of in-situ cell in direction of beam propagation
$\int \epsilon(\tilde{\nu})\mathrm{d}\tilde{\nu}$	**E**:$(1.184 \pm 0.059) \times 10^5\,\mathrm{mol\,l^{-1}}$ **K**:$(1.083 \pm 0.054) \times 10^5\,\mathrm{mol\,l^{-1}}$ **EK**:$(1.192 \pm 0.060) \times 10^5\,\mathrm{mol\,l^{-1}}$	integrated molar absorption coefficient per amino acid (20 °C), determined from transmission measurements [16]
α	$(35 \pm 5)^\circ$	Angle between Amide I' transition dipole moment and helix axis. Literature values vary for instance 30°[17] and 38°[18]

References

[1] F. Niu, R. Schulz, A. C. Medina, R. Schmid and A. Erbe, *Phys. Chem. Chem. Phys.*, 2017, **19**, 13585–13595.

[2] F. Niu, M. Rabe, S. Nayak and A. Erbe, *J. Chem. Phys.*, 2018, **148**, 222824.

[3] J.-J. Max and C. Chapados, *J. Chem. Phys.*, 2002, **116**, 4626–4642.

[4] R. W. Hendler and R. I. Shrager, *J. Biochem. Biophys. Methods*, 1994, **28**, 1–33.

[5] M. Rabe, *J. Open Res. Softw.*, 2020, **8**, 13.

[6] J. E. Crowell and G. Lu, *J. Electron. Spectrosc. Relat. Phenom.*, 1990, **54-55**, 1045–1057.

[7] Y. Chabal, *Surf. Sci.*, 1986, **168**, 594–608.

[8] S. Nayak and A. Erbe, *Phys. Chem. Chem. Phys.*, 2016, **18**, 25100–25109.

[9] S. Rivillon, Y. J. Chabal, F. Amy and A. Kahn, *Appl. Phys. Lett.*, 2005, **87**, 253101.

[10] F. Maroun, F. Ozanam and J.-N. Chazalviel, *J. Phys. Chem. B*, 1999, **103**, 5280–5288.

[11] F. Maroun, F. Ozanam and J.-N. Chazalviel, *Surf. Sci.*, 1999, **427-428**, 184–189.

[12] J.-N. Chazalviel, A. Belaïdi, M. Safi, F. Maroun, B. Erné and F. Ozanam, *Electrochim. Acta*, 2000, **45**, 3205–3211.

[13] N. Hassler, D. Baurecht, G. Reiter and U. P. Fringeli, *J. Phys. Chem. C*, 2010, **115**, 1064–1072.

[14] J.-J. Max and C. Chapados, *J. Chem. Phys.*, 2009, **131**, 184505.

[15] J. H. Burnett, S. G. Kaplan, E. Stover and A. Phenis, Infrared Sensors, Devices, and Applications VI, 2016.

[16] M. Rabe, H. R. Zope and A. Kros, *Langmuir*, 2015, **31**, 9953–9964.

[17] E. Goormaghtigh, V. Raussens and J.-M. Ruysschaert, *Biochim. Biophys. Acta*, 1999, **1422**, 105–185.

[18] D. Marsh, M. Müller and F.-J. Schmitt, *Biophys. J.*, 2000, **78**, 2499–2510.